JOINT EUROPEAN TORUS JET

JET–P(93)82

N. Deliyanakis, D.P. O'Brien, B. Balet, C.M. Greenfield,
L. Porte, A.C.C. Sips, P.M. Stubberfield, H. Wilson

The VH-Mode at JET

The VH-Mode at JET

N. Deliyanakis, D.P. O'Brien, B. Balet, C.M. Greenfield[1],
L. Porte, A.C.C. Sips, P.M. Stubberfield, H. Wilson[2]

JET-Joint Undertaking, Culham Science Centre, OX14 3DB, Abingdon, UK

[1]General Atomics, San Diego, California, USA.
[2]AEA Technology Fusion, Culham, Abingdon, Oxon, OX14 3DB, UK.

Preprint of a paper to be submitted for publication in
Plasma Physics and Controlled Fusion
November 1993

ABSTRACT

The nature and behaviour of the VH-mode, as observed in the JET tokamak, have been investigated; this is a regime of enhanced energy confinement which is often attained during the H-mode phase, following the disappearance of the ELMs. As a result of the high pressure gradients and the high current densities, which develop in an extended region near the separatrix during the VH-phase, a large fraction of the total plasma volume becomes unconditionally stable against ideal and resistive ballooning modes. This effect has been identified as being relevant to the attainment of the VH-mode, but a causal link has not been established. Furthermore, the processes which are responsible for the termination of the VH-mode are not understood.

INTRODUCTION

Some of the high performance JET discharges, in particular those obtained during the campaign of experiments leading up to the preliminary tritium experiment (PTE), make a transition to a regime of enhanced confinement, the VH-mode, after the transition from L- to H-mode. This transition usually coincides with the disappearance of the edge-localized modes (ELMs) observed in the H-mode phase. The VH-mode has been attained in discharges with neutral beam or ion cyclotron heating.

The energy confinement time in this enhanced mode reaches values a factor of 2 above that of the ITER H92-P scaling and a factor of 3 above that of the Goldston L-mode scaling. The high confinement is associated with reduced energy transport near the edge.

During the high confinement phase, a large bootstrap current appears near the edge, associated with the large pressure gradient, and the total current profile broadens. The high edge current results in the coalescence of the first and second regions of stability against ballooning modes, giving unconditional stability, within a substantial fraction of the plasma volume close to the separatrix.

At the onset of confinement degradation, the pressure gradients decrease, as MHD activity increases. However, unconditional stability against ballooning modes is maintained. The termination of the high confinement phase, which is often associated with increased MHD activity, is marked by a high heat flux to the wall, a large influx of impurities and the collapse of the neutron production rate; the enhanced confinement is not recovered after this collapse.

GENERAL BEHAVIOUR OF VH-MODE DISCHARGES

The evolution of four typical PTE discharges is shown in Fig 1(i). Three of these discharges attain the VH-mode, and additional parameters are shown for the VH-phase of one discharge in Fig 1(ii). The plasma parameters and neutral beam power are similar, but pulse 25432 has a double-null instead of a single-null magnetic configuration.

The ELMs that are present in the early phase of the discharges, as manifested by the D_α signal, disappear as the energy confinement time increases above the ITER H92-P value.

Pulse 26087 has been analysed in detail with the transport code TRANSP (Balet et al., 1993).

The local ion diffusivity is reduced at the onset of the ELMs, decreasing further in the VH-phase (fig 2(i)); at the same time, the bootstrap current increases markedly (fig 2(ii)) and the total current profile is consequently broadened. The calculated bootstrap current can exceed the total current near the edge (fig 3(i)), this inference being supported by the measurement of a negative loop voltage. The internal inductance decreases during the VH-mode, reflecting the broadening of the current profile, but starts to increase when the bootstrap current has reached its maximum value (fig 3(ii)).

The ion temperature and the closely connected neutron production rate, which increase during the VH-phase, collapse some 100ms after the confinement time starts to decrease; at the same time, the ion heat flux to the edge increases rapidly; this culminates in dramatically increased impurity content and radiation (carbon bloom).

The $n = 1$ MHD activity is low throughout the ELM and early VH-phase, but increases as the confinement begins to degrade (fig 4). However, it can be seen from this figure that the MHD behaviour varies qualitatively in different VH-mode discharges, so that it is difficult to establish the role played by MHD instabilities in the termination of the VH-mode. A sawtooth crash combined with an ELM is sometimes associated with the termination of the VH-phase. The eventual termination may be due to an internal kink mode, whose computed amplitude is

found to increase with pressure; this mode is exacerbated by the large current density gradient (Nave et al., 1993).

ANALYSIS OF BALLOONING STABILITY

We have investigated the stability of high-performance discharges against the ballooning mode and possible unconditional stability, with the coalescence of the first and second stable regions, using a formulation for finite aspect ratio which has been extended to describe resistive instabilities.

The ideal (non-resistive) ballooning equation for finite aspect ratio (Bishop, 1985) is

$$B_p \frac{d}{dl}\left\{ \frac{|\nabla S|^2}{B^2} B_p \frac{dF}{dl} \right\} + \frac{2\mu_0 p'(\mathbf{B}\times\nabla S)\cdot\mathbf{K}}{B^2} F(l) = 0, \tag{1}$$

where the shear and curvature terms are given by

$$|\nabla S|^2 = \frac{1}{R^2}\left(1 + \frac{I^2}{R^2 B_p^2}\right) + I^2 R^2 B_p^2 P^2(l,l_0), \tag{2}$$

$$(\mathbf{B}\times\nabla S)\cdot\mathbf{K} = \frac{I^2 \sin u}{R^4 B_p} - \frac{B_p}{RR_c} - \frac{I^2 B_p}{B}\frac{\partial B}{\partial l} P(l,l_0), \tag{3}$$

with

$$P(l,l_0) = \int_{l_0}^{l} \frac{dl}{R^2 B_p}\left[\frac{I'}{I}\left(1 + \frac{I^2}{R^2 B_p^2}\right) + \frac{\mu_0 p'}{B_p^2} + \frac{2}{RB_p R_c}\left(1 + \frac{R_c \sin u}{R}\right)\right]; \tag{4}$$

In the equations above, $p(\psi)$ is the pressure function, $I(\psi)$ is the current flux function, primes denote differentiation with respect to the flux function ψ, R is the major radius, R_c is the radius of curvature, B_p is the poloidal field, B is the total field and u is the angle between the tangent to the flux surface and the major radius; dl is an arc length element defined in the clockwise direction, so that

$$dl = -h d\theta, \tag{5}$$

where θ is the poloidal angle and h is the flux surface metric. The integrand of $P(l,l_0)$ corresponds to the local shear. l_0 is an undefined parameter that must be set to the value that corresponds to the most unstable mode (Connor, Hastie and Taylor,

1979). Treating p' as an eigenvalue with eigenfunction $F(l)$, the ballooning equation is solved subject to a vanishing eigenfunction in the limit of large l, to find the pressure gradient values corresponding to marginal stability.

In the dimensionless form of the ballooning equation, one defines a *current density parameter*

$$\Lambda = \frac{\varepsilon_n I}{B_n} \left< \frac{\mu_0 \mathbf{J} \cdot \mathbf{B}}{B^2} \right> = - \frac{\varepsilon_n}{B_n} \left(II' + \mu_0 p' I^2 < 1/B^2 > \right), \tag{6}$$

and a *pressure gradient parameter*

$$\alpha = - \frac{2\mu_0 r_n^2 p'}{B_n}, \tag{7}$$

where the subscript n refers to a normalization value, which is here taken to be the value at the inner equatorial plane (i.e. at $\theta = \pi$). It should be noted that, for a given flux surface geometry, the shear parameter s is linearly related to these two parameters. For a given flux surface and value of Λ, one can solve the ballooning equation to obtain the two eigenvalues α_L and α_U that correspond to the lower and upper stability limits. For the first and second stability region, one has $\alpha < \alpha_L$ and $\alpha > \alpha_U$, respectively; the value of α_L has only a weak dependence on the parameter l_0. These limits can be compared with the experimentally determined α value. As Λ is increased on a given flux surface, when the surface-averaged current increases, the lower and upper eigenvalues approach one another, until, eventually, the unstable region vanishes and the two stable regions coalesce, at a critical value Λ_{crit}. A similar behaviour is observed as flux surfaces close to the separatrix are approached.

In order to investigate the resistive case, we use a two-scale asymptotic expansion of the solution $F(\theta)$ (Wilson, 1990 and 1991), valid in the limit of large poloidal angle, as follows:

$$\lim_{\theta \to \pm\infty} F(\theta) = F_L(\theta) + \Delta' F_S(\theta), \tag{8}$$

where F_L and F_S are large and small series expansions in powers of $1/|\theta|$, which can be determined from the ballooning equation. Δ' is a parameter representing the degree of resistivity: It is large in the ideal limit, but decreases with increasing resistivity. The relevant value of Δ' depends on the pertaining unstable mode (Drake and Antonsen,

1984), but can be determined only from the complete set of resistive ballooning equations.

Making use of the fact that resistivity and inertia become important only at large values of the independent ballooning transformed variable, we solve the ideal ballooning equation as an initial-value problem for fixed α, obtaining two linearly independent solutions, which are then matched to the asymptotic expansion giving Δ'_R (for $l \to +\infty$) and Δ'_L (for $l \to -\infty$); the boundary condition $\Delta'_R = \Delta'_L$ fixes the eigenfunction gradient $F'(0)$, as well as the Δ'-value corresponding to the chosen α-value. One finds that Δ' increases extremely rapidly as α approaches the ideal limit. It follows that, for values of $\Delta' > 1$, these being relevant to JET discharges, the lower stability limit α_L is close to its ideal limiting value, as shown in Fig 5. The unstable region increases only slightly for such cases; in particular, the point of coalescence is not significantly altered by the inclusion of resistivity. Although the inclusion of resistivity does result in a larger unstable region (with a lower stability limit), it is not clear whether the edge is unstable against resistive ballooning modes during the ELM-phase that precedes the VH-phase.

BALLOONING STABILITY IN THE VH-MODE

The geometrical quantities necessary for the solution of the ballooning equation are obtained from the magnetic equilibrium codes IDENTC or EFIT. Near the edge of the plasma ($\overline{\psi} \geq 0.85$), the pressure and pressure gradient are calculated from the density and temperature profiles obtained, respectively, from the microwave reflectometer and the heterodyne radiometer; both diagnostics provide good spatial resolution near the edge, allowing large density and temperature gradients to be measured with confidence. These data are supplemented by corresponding data from the LIDAR Thomson scattering diagnostic, which have lower spatial and temporal resolution, but extend over the entire plasma cross-section. The total pressure is assumed to be twice the electron pressure for the purposes of this analysis (As the ion temperature is higher than the electron temperature, this is likely to be an underestimate). The processed reflectometer measurements give the major radii for a range of electron densities, leading to density profiles that can be many-valued; these have to be converted to single-valued, monotonic profiles, and this process can introduce some uncertainty in the pressure gradient. The reflectometer data are further limited by the fact that profile processing is currently impossible during phases

with ELM activity, so that it is not clear whether the ELMs are due to the ballooning mode.

These uncertainties notwithstanding, we have established that, during the VH-mode, the pressure gradients and bootstrap current can be large enough for the coalescence of the two stable regions ($\Lambda > \Lambda_{crit}$), thus leading to unconditional stability against ballooning modes. Although the edge current is low during the ELM phase and the second stability region is inaccessible, high edge currents develop rapidly at the end of the ELM phase and persist during the VH-mode; these high currents are sufficient for coalescence, as shown in Fig 6(i) for pulse 26087. At the same time the edge pressure gradient increases dramatically, moving into the second stable region, as shown in Fig 6(ii); this unconditional stability is lost soon after the time of maximum neutron production rate at 13.4s. The plasma volume where unconditional stability is obtained increases steadily, from the edge inwards, during the VH-mode, as shown in Fig 7 for pulse 25264. This effect can also be seen from the temporal evolution of the pressure gradient distribution near the edge, shown in Fig 8 for pulse 26095. It is evident that the edge pressure gradient increases at the onset of the VH-mode at 12.7s, and the region of high gradient subsequently expands inwards; the high edge gradient in this case collapses at 14s, just after the termination of the VH-mode.

The pressure gradients decrease abruptly at about the same time as the enhanced energy confinement time decreases, which is then followed by a dramatic decrease in the fusion yield; the unstable region then re-appears and the unconditional stability is lost. We conclude that the enhanced confinement in the VH-phase is correlated with the broadening of the region of high gradients associated with the H-mode, and with the disappearance of the ballooning stability limit. However, we are unable to establish a causal link between these observations.

COMPARISON BETWEEN JET AND DIII-D VH-MODES

The VH-mode was first observed on the DIII-D experiment, following the boronization of the vessel (Jackson et al., 1991); a detailed comparison of the JET and DIII-D VH-modes has been carried out (Greenfield et al., 1993).

Whereas an ELM phase is observed in JET before the transition to the VH-mode, no such activity is observed in DIII-D, the transition occuring during the ELM-free H-mode. It should also be noted that, because of their more favourable shape (higher

triangularity), DIII-D edge plasmas are unconditionally stable against ballooning modes before, as well as during, the VH-phase.

It has also been observed on DIII-D that, at the transition to the VH-mode, the toroidal rotation increases within the flux surface with $\rho = 0.6 - 0.8$ and decreases outside, leading to a steep toroidal rotation profile. This change is associated with the broadening of a region of high radial electric field shear, and occurs before the improvement in the confinement. Theory shows that the increased radial electric field shear can lead to improved confinement by stabilizing the turbulence (Staebler et al., 1993). This effect of increased toroidal rotation has not been observed on JET: Some discharges that attain a VH-mode exhibit a continuous increase in toroidal rotation, in contrast to some discharges without a VH-mode (Greenfield et al., 1993). It is important to note, however, that the VH-mode has been attained on JET in discharges with *only* ion cyclotron heating (e.g. pulse 25264), in which there is little or no rotation. One concludes that the increased toroidal rotation and the associated enhanced radial electric field shear may not be relevant to the attainment of the VH-mode (it should nevertheless be noted that the electric field shear can also be driven by pressure gradient; Staebler et al., 1993).

These differences notwithstanding, the energy confinement times in both experiments can reach values a factor of 2 above those predicted by the JET/DIII-D H-mode scaling. The behaviour of the two experiments and in particular the local transport effects described above are similar, once the VH-mode has been established. It should finally be noted that a discharge on DIII-D sharing similar parameters and plasma shape with the JET discharges exhibited very similar behaviour in all respects: in particular, the VH-phase was preceded by a phase with ELM activity, and unconditional stability against ballooning modes was obtained at the start of the VH-phase.

CONCLUSIONS

A regime of very high confinement, the VH-mode, has been observed on JET; this is associated with an ELM-free phase that follows the ELM phase of the H-mode, and is characterized by a high energy confinement time.

The VH-mode is associated with a broadening of the region of high pressure gradient of the H-mode, as well as with a substantial increase of the edge pressure gradient and the bootstrap current.

The high current density in the edge results in a large fraction of the plasma becoming unconditionally stable against ballooning modes. This effect may be responsible, or at least necessary, for the improved confinement of the VH-mode. The confinement degradation and eventual termination of the VH-mode are often associated with MHD activity, whose role is not clear.

REFERENCES

Balet, B., et al. (1993) *Particle and Energy Transport during the First Tritium Experiments on JET*, JET Report JET-P(93)18, to be published in Nucl. Fusion., MS no 5595.

Bishop, C.M. (1985) *Construction of Local Axisymmetric MHD Equilibria*, Culham Laboratory Report CLM-R249.

Connor, J.W., Hastie, R.J. and Taylor, J.B. (1979) Proc. Roy. Soc., **A365**, 1.

Drake, J.F. and Antonsen, T.M. (1984) Phys. Fluids, **28**, 544.

Greenfield, C.M., et al. (1993) *Investigations of VH-mode in DIII-D and JET* (Invited paper, 20th EPS Conference on Controlled Fusion and Plasma Physics, Lisbon, 1993), GA Report GA-A21368 and JET Report JET-P(93)75, to be published in Plasma Phys. Contr. Fusion.

Jackson, G.L., et al. (1991) Phys. Rev. Lett., **67**, 3098.

Nave, M.F.F., et al. (1993) *MHD Activity in JET High Performance Discharges*, Proc 20th EPS Conference on Controlled Fusion and Plasma Physics, Lisbon, **17C**, I-191.

Staebler, G.M., et al. (1993) *H and VH Modes from Energy, Particle and Momentum Transport Models*, GA Report GA-A21278, submitted to Phys. Fluids.

Wilson, H.R. (1990) Plasma Phys. Contr. Fusion, **32**, 443.

Wilson, H.R. (1991) Plasma Phys. Contr. Fusion, **33**, 221.

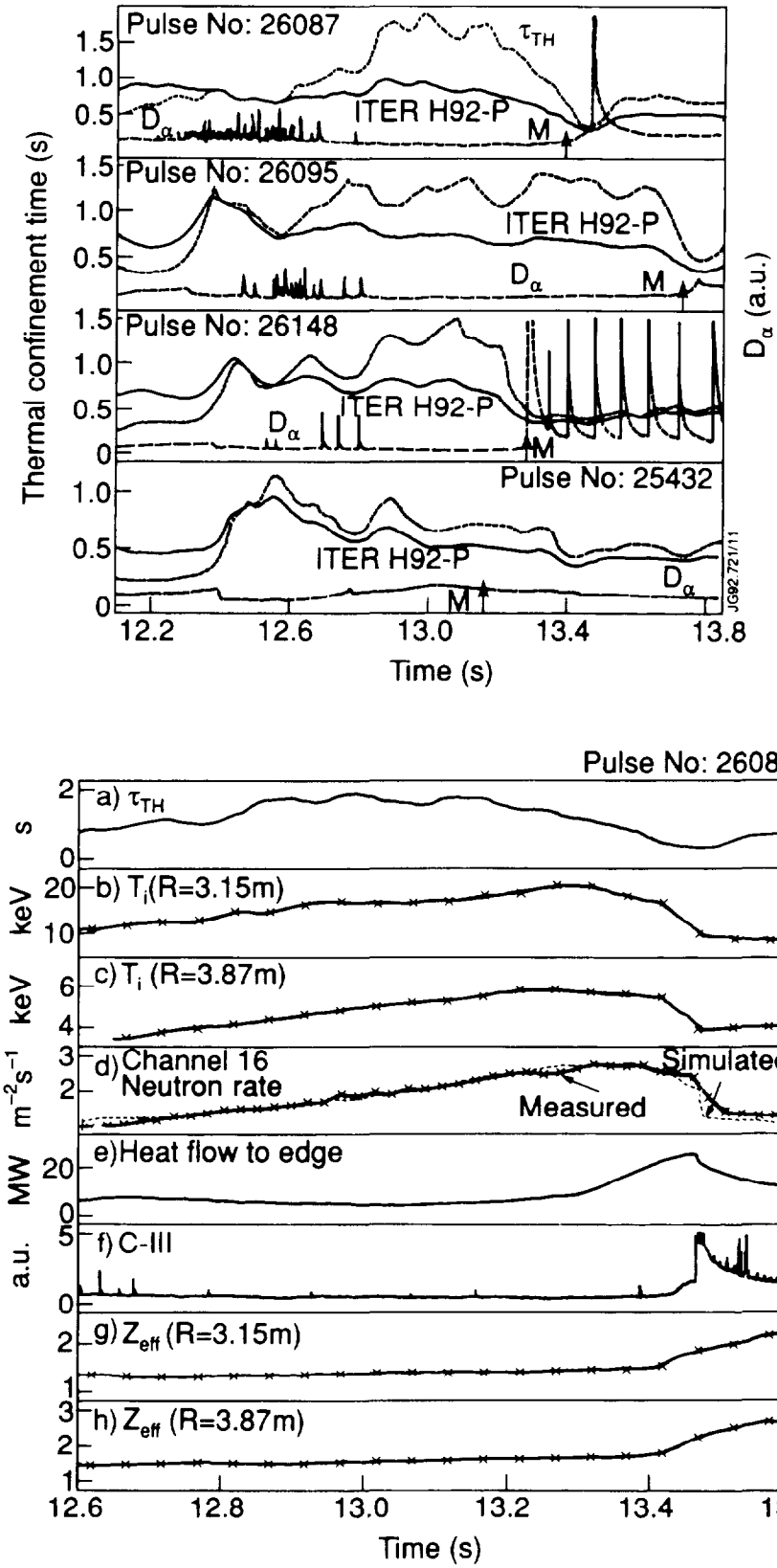

Fig 1: Evolution of PTE discharges: (i) thermal energy confinement time compared to ITER H92-P scaling, and edge D_α emission for four discharges, the first three of which attain VH-mode (M indicates the times of maximum neutron production); (ii) thermal energy confinement time (a), central (b) and edge (c) ion temperatures, neutron production rate (d), edge ion heat flux (e), edge C-III emission (f), central (g) and edge (h) effective charge, for pulse 26087.

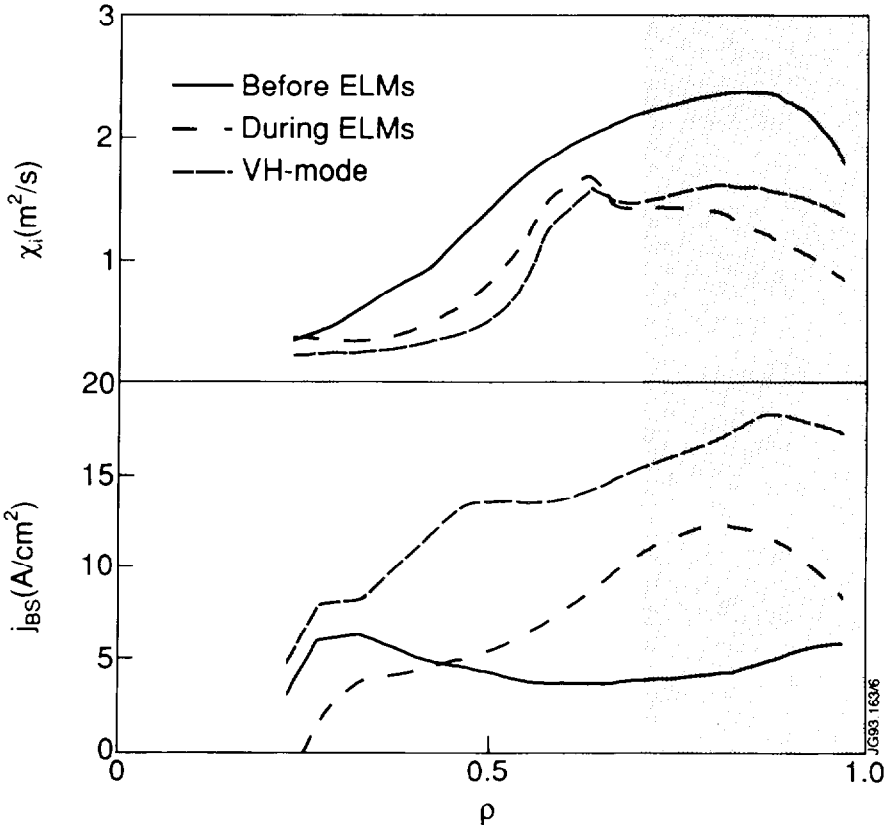

Fig 2: Changes in profiles of (i) ion diffusivity and (ii) bootstrap current density, before and during the ELM phase and during the VH-mode.

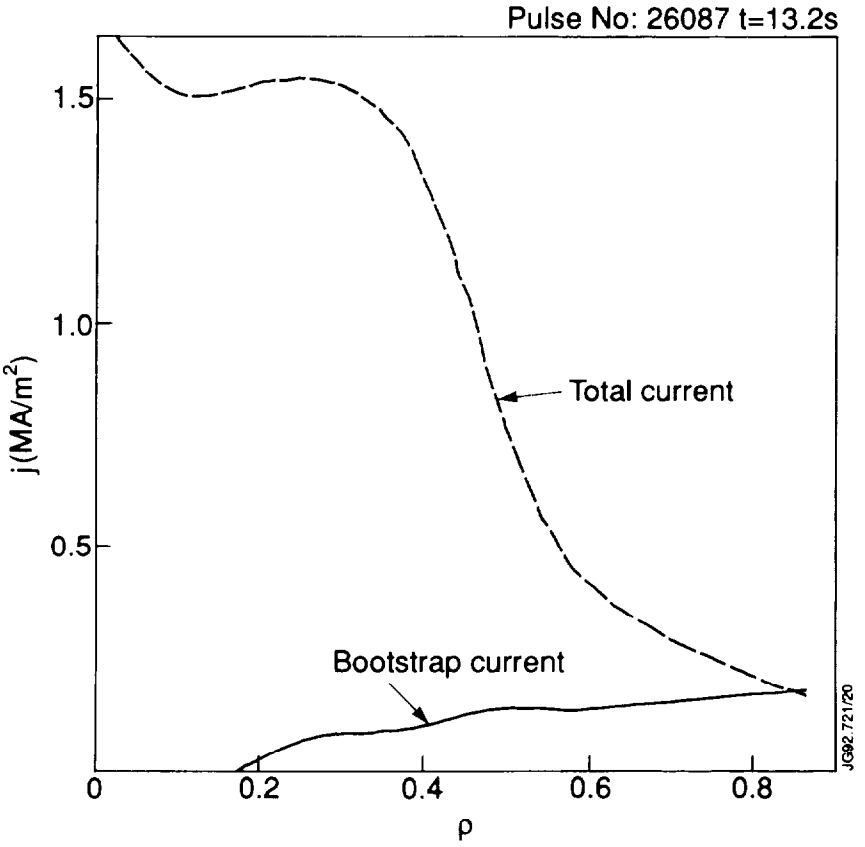

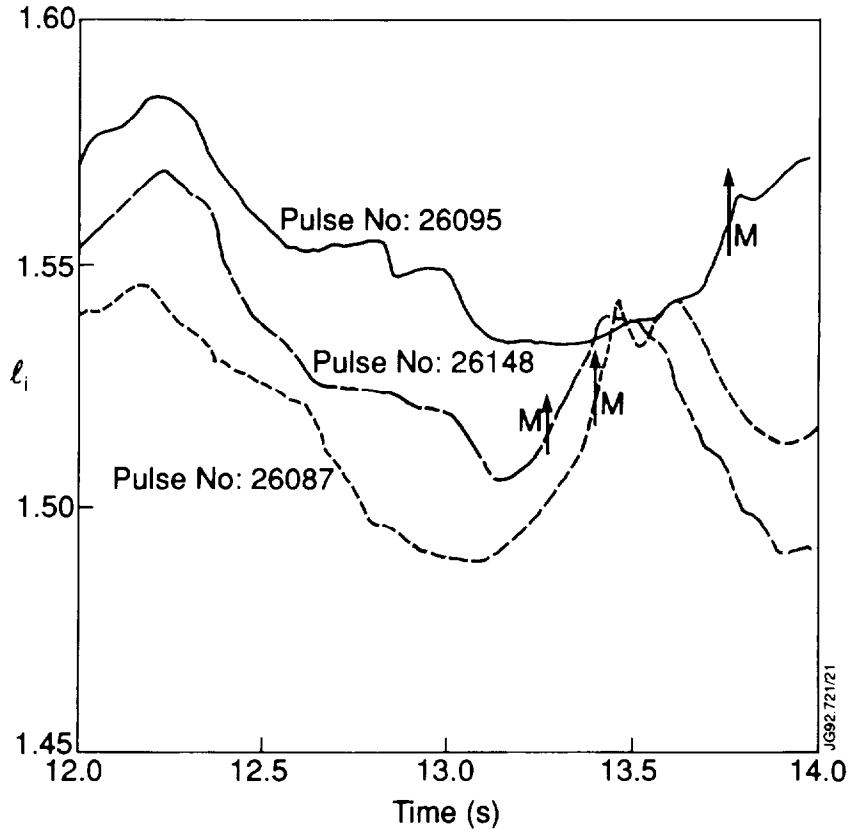

Fig 3: (i) Profiles of total and bootstrap current densities, at the time of maximum bootstrap current; (ii) evolution of internal inductance (M indicates the times of maximum neutron production).

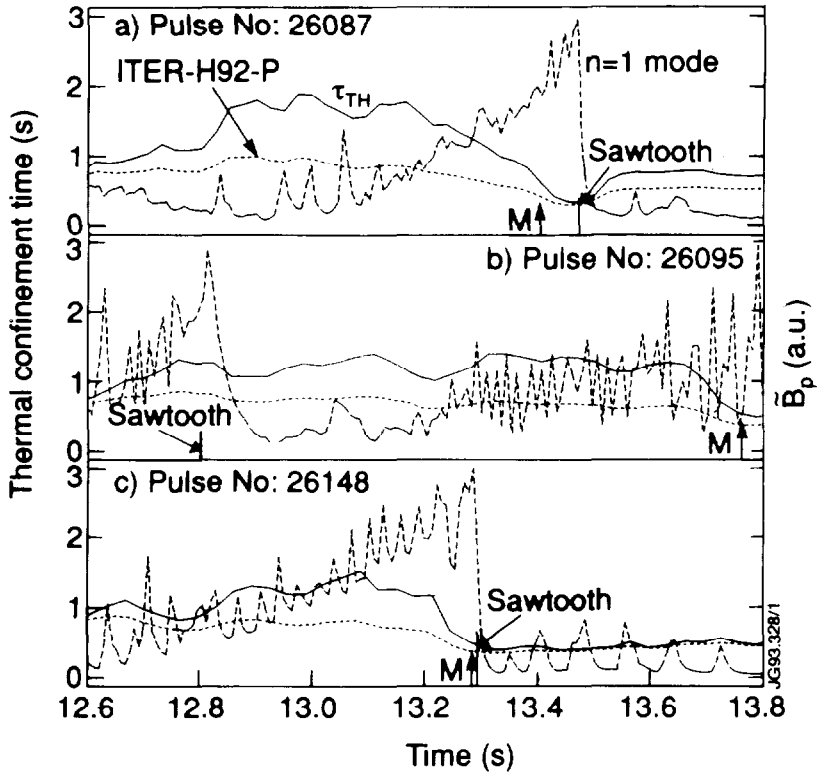

Fig 4: Evolution of $n = 1$ MHD activity and thermal energy confinement time.

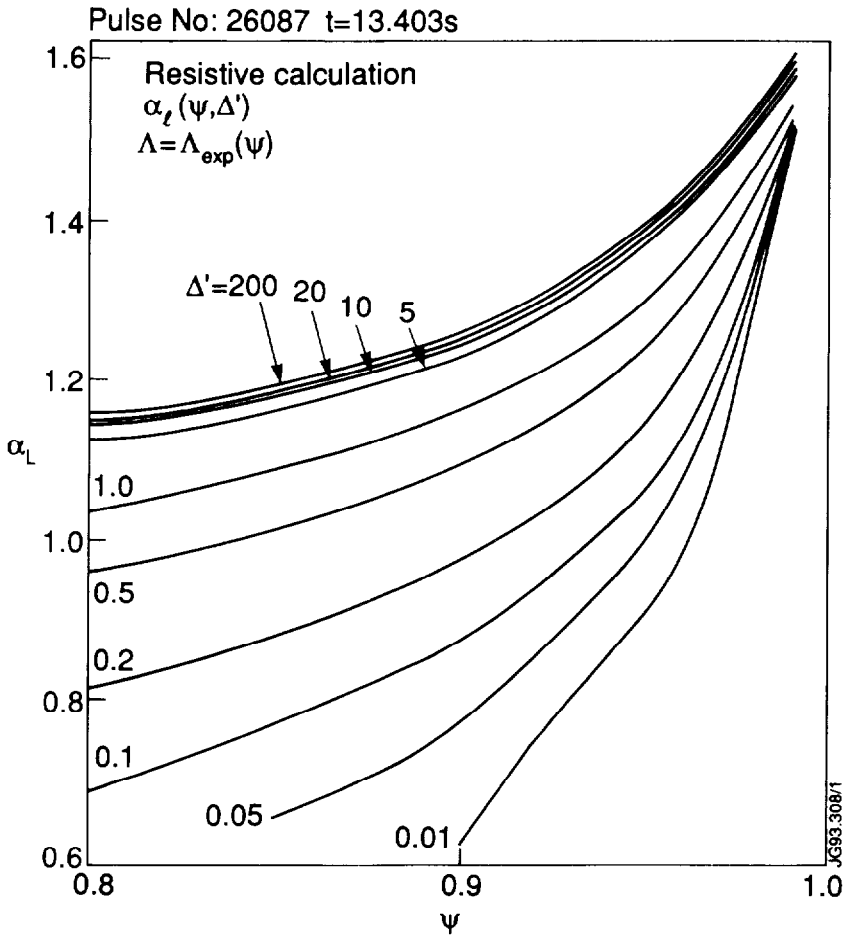

Fig 5: Lower stability boundaries for different values of resistivity parameter Δ', for pulse 26087 at the termination of the VH-phase.

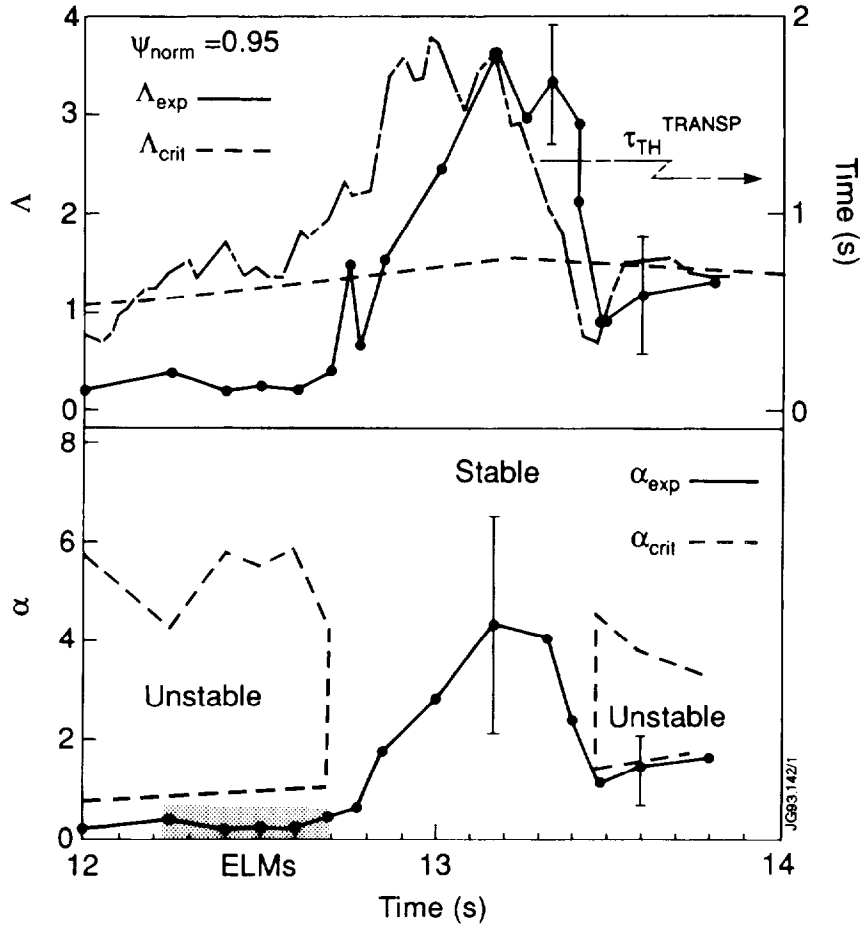

Fig 6: Evolution of (i) experimental and critical Λ, and confinement time; (ii) experimental pressure gradient α with stability boundaries, for pulse 26087. The ELM phase, during which reflectometer data are not available, is shaded.

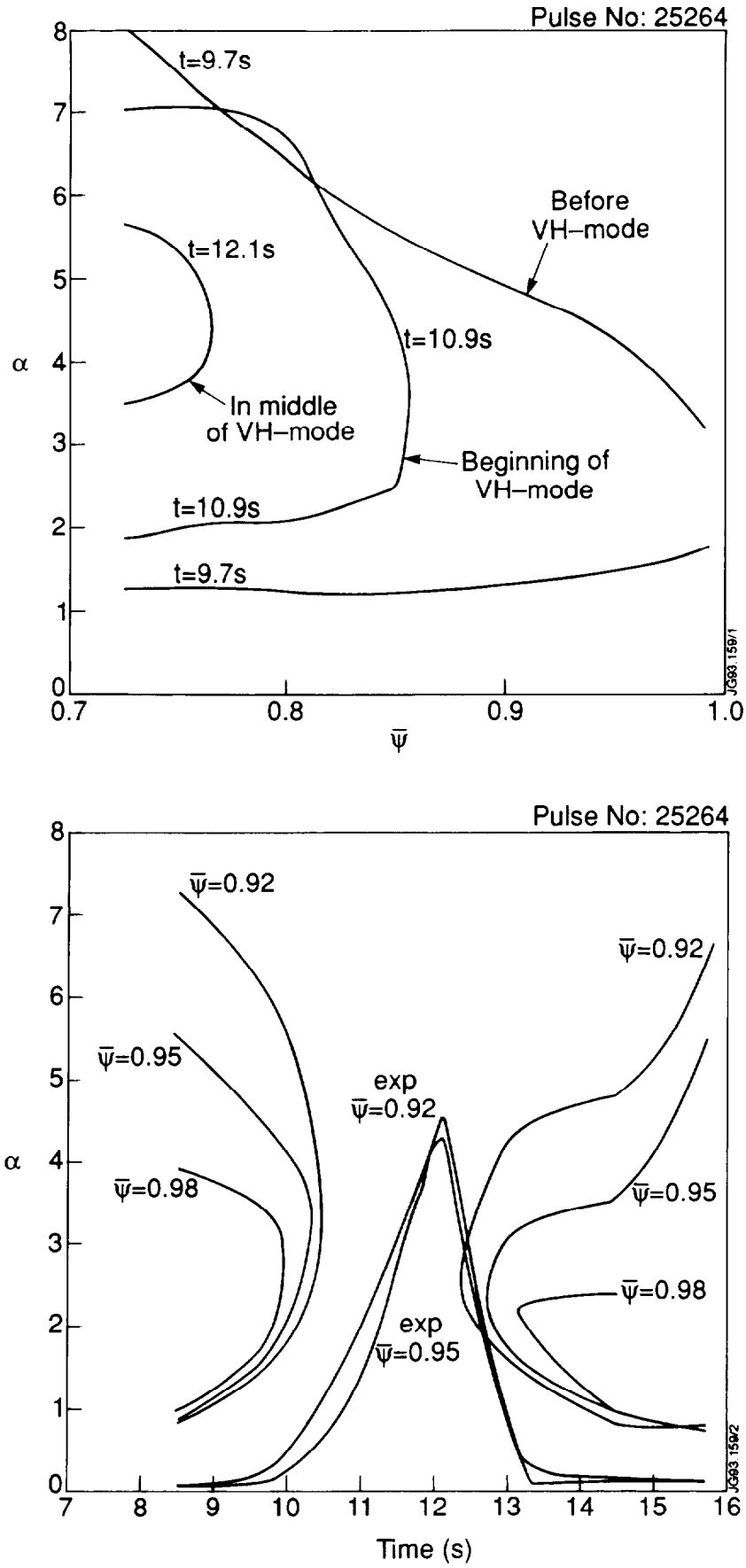

Fig 7: (i) Region with unconditional stability increases inwards, reaching more than 30% of plasma volume; (ii) evolution of experimental pressure gradient and stability boundaries, for pulse 25264.

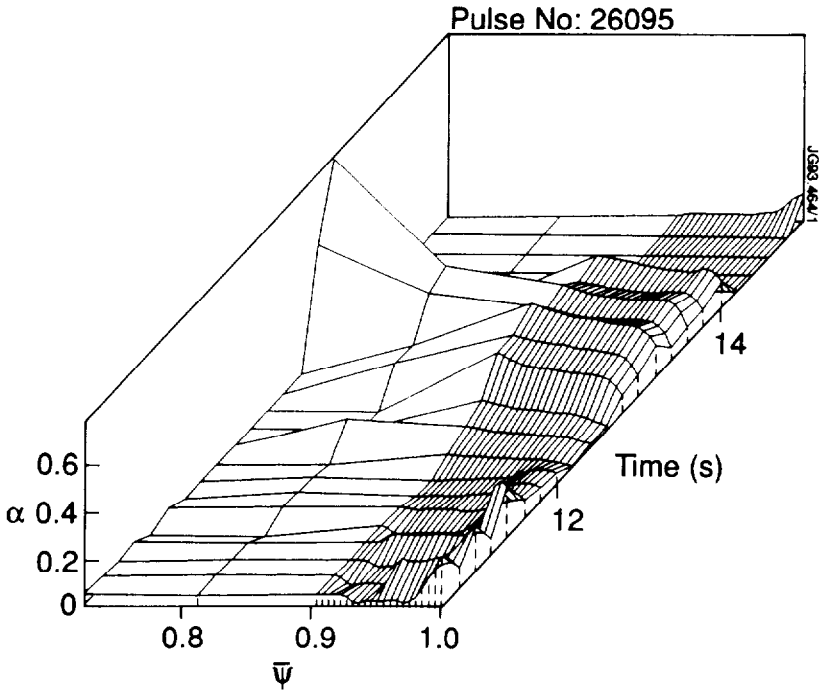

Fig 8: Evolution of normalized edge pressure gradient, for pulse 26095.